JOURNAL OF GEOPHYSICAL RESEARCH, VOL. 90, NO. A8, PAGES 7457-7469, AUGUST 1, 1985

Subionospheric VLF/LF Phase Perturbations Produced by Lightning-Whistler Induced Particle Precipitation

U. S. INAN, D. L. CARPENTER, R. A. HELLIWELL, AND J. P. KATSUFRAKIS

Space, Telecommunications and Radioscience Laboratory, Stanford University, California

New evidence of phase perturbations of subionospheric VLF/LF signals, produced by lightning-whistler-induced precipitation of bursts of radiation belt electrons, is reported. Phase changes of 0.1–1.0 μs on a 12.9-kHz signal arriving at Palmer, Antarctica ($L \sim 2.4$), over a $\sim$ 2400-km path are regularly observed with a characteristic signature of a rapid ($\leq$ 1 s) onset followed by a relatively slow (10–30 s) recovery. Event occurrence peaks during equinoctial periods, with typical rates of 1–40 events per hour lasting for several hours per night. The observed phase perturbations can be interpreted to correspond to a rapid reduction of up to $\sim$0.1–1.0 km in the effective nighttime ionospheric reflection height ($\sim$ 85 km) for the subionospheric VLF signals. The incident energetic particle fluxes that are required to produce the extra ionization are estimated to be $\sim 10^{-3}$–10^{-2} ergs cm^{-2} s^{-1}. Such flux levels are generally consistent with those estimated using theoretical models of whistler-particle resonant scattering as well as direct satellite-based observations of whistler-induced precipitation. This phenomenon provides a sensitive means for detecting wave-induced burst particle precipitation. The ionospheric perturbations resulting from such precipitation may cause significant errors in certain global navigation aids, such as the Differential Omega and LORAN-C systems.

1. INTRODUCTION

Rapid phase perturbations of subionospherically propagating VLF/LF signals are known to be associated with lightning-generated whistlers that propagate in the magnetosphere [*Helliwell et al.*, 1973; *Lohrey and Kaiser*, 1979; *Carpenter et al.*, 1984]. The perturbations, called "Trimpi events" or "Trimpi effects" after their discoverer, are attributed to alterations in the earth-ionosphere waveguide caused by localized enhancements in the ionospheric D region [*Helliwell et al.*, 1973]. These enhancements are produced by bursts of high-energy (> 40 keV) electrons that are precipitated out of the earth's radiation belts by the whistler waves.

The process believed to be responsible for Trimpi events is described in Figure 1. An atmospheric lightning discharge generates electromagnetic wave energy over a broad range of frequencies. Typically, energy in the ELF/VLF range (300 Hz to 30 kHz) is coupled into the magnetosphere and propagates between hemispheres in the whistler mode [*Helliwell*, 1965]. In the magnetosphere, cyclotron resonant interactions between the whistler wave and counterstreaming trapped radiation belt electrons can occur [*Brice*, 1964]. One result of this interaction is wave-induced pitch angle scattering and the associated reduction in mirror altitude of the resonant particles, leading to their precipitation into the ionosphere [*Dungey*, 1963]. Through collisions with the ionospheric constituents, the precipitated electrons may cause localized ionization and conductivity enhancements, heating, visual and ultraviolet light emissions and bremmstrahlung x rays [*Rees*, 1969]. When the ionization enhancements extend below $\sim$ 90 km into the D region, there may occur measurable amplitude and phase perturbations of VLF/LF electromagnetic radio signals that propagate in the nighttime earth-ionosphere waveguide. Such changes consist of fast ($\sim$ 1 s) amplitude increases or decreases of $\sim$1–3 dB, and/or phase changes of a few microseconds, followed by a $\sim$ 30-s recovery to pre-event levels. An example of typical amplitude changes on a 37.2-kHz signal is shown in Figure 1*c*.

The first observations of whistler-associated amplitude perturbations of the kind described above were reported by *Helliwell et al.* [1973]. More recent results have shown that Trimpi events can be observed at mid- to low latitudes ($L \leq 3$) within the plasmasphere [*Carpenter and LaBelle*, 1982], that these lightning-induced perturbations are much more common than previously believed [*Leyser et al.*, 1984], and that perturbations can be observed on signals in the LF and MF frequency range (e.g., 800 kHz) [*Carpenter et al.*, 1984]. Events were also observed at higher latitudes ($L \geq 3.5$), near to and poleward of the plasmapause, in association with whistlers and whistler-triggered noise bursts [*Dingle and Carpenter*, 1981; *Carpenter et al.*, 1985]. These indirect indications of whistler-induced precipitation and its ionospheric effects have recently been supported by direct satellite-based observations of bursts of precipitating particles in one-to-one association with lightning-generated whistlers observed at a ground station [*Voss et al.*, 1984].

The purpose of this paper is to present and discuss new evidence of whistler-associated phase perturbations of subionospheric signals. Events of this type, called phase Trimpi's, were first reported by *Lohrey and Kaiser* [1979]. A brief initial report on phase perturbations of 12.9-kHz Omega Argentina, navigation signals observed at Palmer Station, Antarctica, was presented by *Carpenter et al.* [1984], and initial examples of phase Trimpi's on Siple transmitter signals received at South Pole and Palmer Stations were shown by *Carpenter et al.* [1985]. In this paper we present and briefly discuss occurrence statistics in terms of the seasonal distribution and hourly rate of events. We also present a first-order quantitative interpretation of individual events in the context of (1) a model of magnetospheric whistler-induced electron precipitation [*Chang and Inan*, 1983]; (2) commonly accepted models of the resulting D region density

Paper number 5A8537.
0148-0227/85/005A-8537$05.00

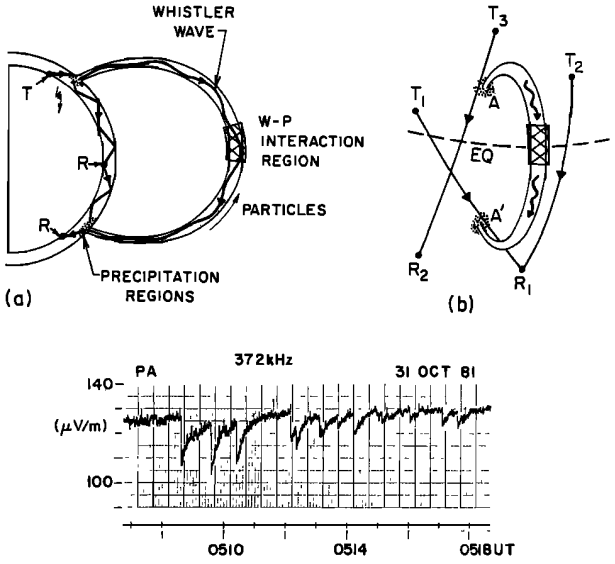

Fig. 1. Illustration of the detection of lightning-induced precipitation by means of associated subionospheric signal perturbations, i.e., the "Trimpi" effect; (*a*) meridional plane projection of the field line of propagation showing a whistler wave launched by a lightning discharge and a subionospheric VLF/LF/MF signal propagation path from a transmitter (T) to receivers (R), (*b*) a three-dimensional sketch showing the spatial relationship of a whistler mode duct and subionospheric signal paths between transmitters (T_1, T_2, T_3) and receivers (R_1, R_2) that cross the corresponding precipitation regions (A, A'), (*c*) chart recording showing Trimpi events as amplitude perturbations on a 37.2-kHz signal, originating in southern California (see Figure 2) and observed at Palmer Station, Antarctica. The characteristic rapid onset (~ 1 s) and the relatively longer recovery (~ 30 s) times are clearly evident.

enhancements [*Rees*, 1969]; and (3) a model of VLF propagation in the earth-ionosphere waveguide [*Wait and Spies*, 1964]. We then discuss the observed phase changes as a possible source of error in global navigation systems that rely on phase coherent subionospheric VLF/LF transmissions.

The possible role of lightning-generated whistlers in the loss of radiation belt particles was suggested two decades ago [*Dungey*, 1963; *Cornwall*, 1964]. Recent findings about Trimpi effects, in particular their relatively high occurrence rate at ≤ 2.4 [*Leyser et al.*, 1984], have strengthened interest in this question. Direct satellite observations of whistler-induced electron precipitation have provided striking new evidence of the role of lightning in particle loss from the belts [*Voss et al.*, 1984]. A statistical study of precipitation of electrons with energy $\geq$ 65 keV observed on a low-altitude satellite has indicated that at $L \leq 2.5$, the effect of precipitation induced by whistlers and/or man-made waves may be significant [*Imhof et al.*, 1984]. A theoretical model study of whistler-induced precipitation has also indicated that the latitude range $2 \leq L \leq 3$ may be a preferred region for lightning-induced precipitation of $\geq$ 40-keV electrons [*Chang and Inan*, 1985].

These recent findings raise questions about the role of lightning and thunderstorms in the internal coupling processes of the atmosphere-ionosphere-magnetosphere system. While the results show direct evidence of the removal of electrons from the radiation belts by lightning discharges in single events, the effect of whistler-induced precipitation on the overall loss rates of trapped electrons is not known. In particular, the relative importance of whistlers with respect to other wave phenomena (e.g., plasmaspheric hiss) has yet to be determined. Further information on the geographic distribution of Trimpi events and the spatial extent and intensity of the wave-induced precipitation fluxes is needed in order to answer this question.

Certain effects of energetic particle precipitation on wave propagation in the earth-ionosphere waveguide have been extensively documented. For example, at high and mid- to high latitudes, associations between phase perturbations of subionospheric radio signals and minutes-long particle precipitation events connected with substorms and bursts of solar particles are well established [e.g., *Potemra et al.*, 1967, 1969; *Potemra and Rosenberg*, 1973; *Westerlund and Reder*, 1973; *Kikuchi and Evans*, 1983]. Effects at mid- to low latitudes have also been reported [*Doherty*, 1971]. In such studies, the precipitation events were not directly associated with magnetospheric waves, although the possible role of waves was discussed in a substorm-related case [*Potemra and Rosenberg*, 1973]. The results of *Doherty* [1971] are remarkably similar to those reported in this paper, in terms of the burst nature of the reported phase changes and the seasonal and latitudinal distributions of occurrence.

In contrast to these earlier observations, the whistler-associated burst precipitation events can yield explicit information on the scattering waves. The characteristic temporal signature of the ionospheric effects can be used in the quantitative modeling of the effect. In addition, interpretive modeling of the overall process can be based in specific cases upon measurements of the whistler path L values, equatorial electron density, apparent duration of the precipitation bursts, and time relationships between the arrival of the magnetospheric whistler and the time of occurrence of the subionospheric signal perturbation.

In the following we present examples recorded at Palmer Station, Antarctica, of phase perturbations on various VLF/LF signals and occurrence statistics of perturbations on 12.9-kHz signals from the Omega Argentina transmitter (43°S, 65°W). Following a brief discussion of the occurrence data, we present a first-order quantitative model of an individual event. A final section on the implications of our results in the context of global VLF/LF navigation is followed by a summary of the results and conclusions.

2. Experimental Results

Data Acquisition

The data described here were acquired at Palmer Station, Antarctica (65°S, 64°W, $L \simeq 2.4$), during 1983. The geometry of the observations and sample subionospheric signal paths that were monitored are shown in Figure 2. The locations of the various signal sources and their operating frequencies are given in Table 1.

The data were recorded on eight-channel Sanborn charts and on magnetic tapes. The charts include amplitude records of signals from a number of transmitters, the phase of one signal, and integrated VLF intensity in the frequency bands 0.5–1.0 kHz and 2.0–4.0 kHz. Trimpi events were identified by inspecting the charts for both the characteristic perturbation signature, as shown in Figure 3*a*, as well as

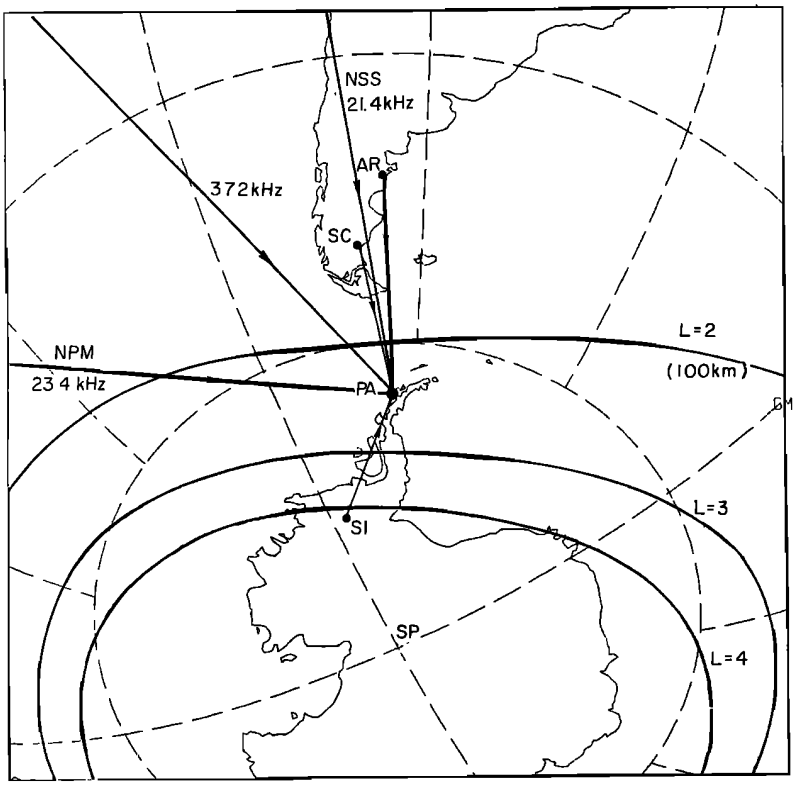

Fig. 2. Map showing examples of great circle paths from various signal sources to Palmer (PA) and Siple (SI) stations, Antarctica.

a time correlation of the events with whistlers, shown in Figure 3*b* as spikes on a record of integrated 2- to 4-kHz VLF amplitude. Representative examples of correlated whistlers are indicated in Figure 3*b* by arrows.

The magnetic tapes contain broadband VLF recordings (0–30 kHz) for one 10-min or 12-min period each hour throughout the local night (typically 0150-1000 UT during March/April). Amplitude and phase recordings of selected transmitter signals were recorded on a separate track as voltage-controlled oscillator outputs. The data from magnetic tapes were used for measurements of the correlated whistlers and for high-time resolution measurements of the VLF/LF signal phase perturbations.

Time Signature of Phase Changes and Association With Magnetospheric Whistlers

Some details of the correlation illustrated in Figure 3 are shown in Figure 4. The top panel shows a voltage-controlled oscillator (VCO) record of the 12.9-kHz phase on a linear scale, while Figure 4*b* shows the corresponding 0- to 10-kHz frequency-time spectrum. Marks above Figure 4*b* show the times of origin of three strong whistlers that coincided with three rapid phase advances of ~0.5 μs. (Phase advances (Δt) are conventionally expressed in units of time (microseconds). For a wave at a frequency ω, the corresponding phase charge in radians is $\Delta\phi = \omega\Delta t$.) The first event is shown on expanded records in Figures 4*c* and 4*d*; the time of origin of the lightning stroke that generated the whistler is marked by an arrow below Figure 4*d*. The observed delay between the time of the discharge and the onset of the phase perturbation was ~ 0.5 s; this is illustrated in high-time resolution records of another event shown later in the interpretation section.

The phase record of Figure 4 was obtained using a phase tracking receiver and an integration time constant of ~ 1.5 s. This integration time was found to be sufficient for identification of events on continuous chart recordings. The 12.9-kHz Omega Argentina signal has a duty cycle of ~ 40%, consisting of two pairs of ~ 1-s pulses, with the pairs separated by intervals of ~ 1.5 s and ~ 4 s within a basic repetition cycle of 10 s. The times of reception of Omega pulses at Palmer are indicated at the bottom of Figures 4*a* and 4*d*. In order to ensure the continuity of phase during the off periods, a holding circuit was utilized. The sawtooth nature of the phase record in Figure 4*a* is due to the slow drift of the phase during such off periods.

The characteristic signature of Trimpi events, i.e., a rapid onset followed by a relatively slow (10-100 s) recovery, is

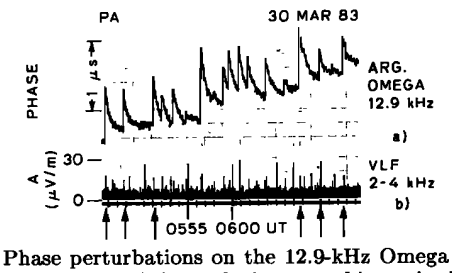

Fig. 3. Phase perturbations on the 12.9-kHz Omega Argentina signal. The lower panel shows the integrated intensity in the 2- to 4-kHz band where individual whistlers appear as "spikes." The observed phase advances are generally correlated with whistlers, several of which are indicated by arrows. The spikes at 0550, 0555, 0600, etc., are due to a calibration signal.

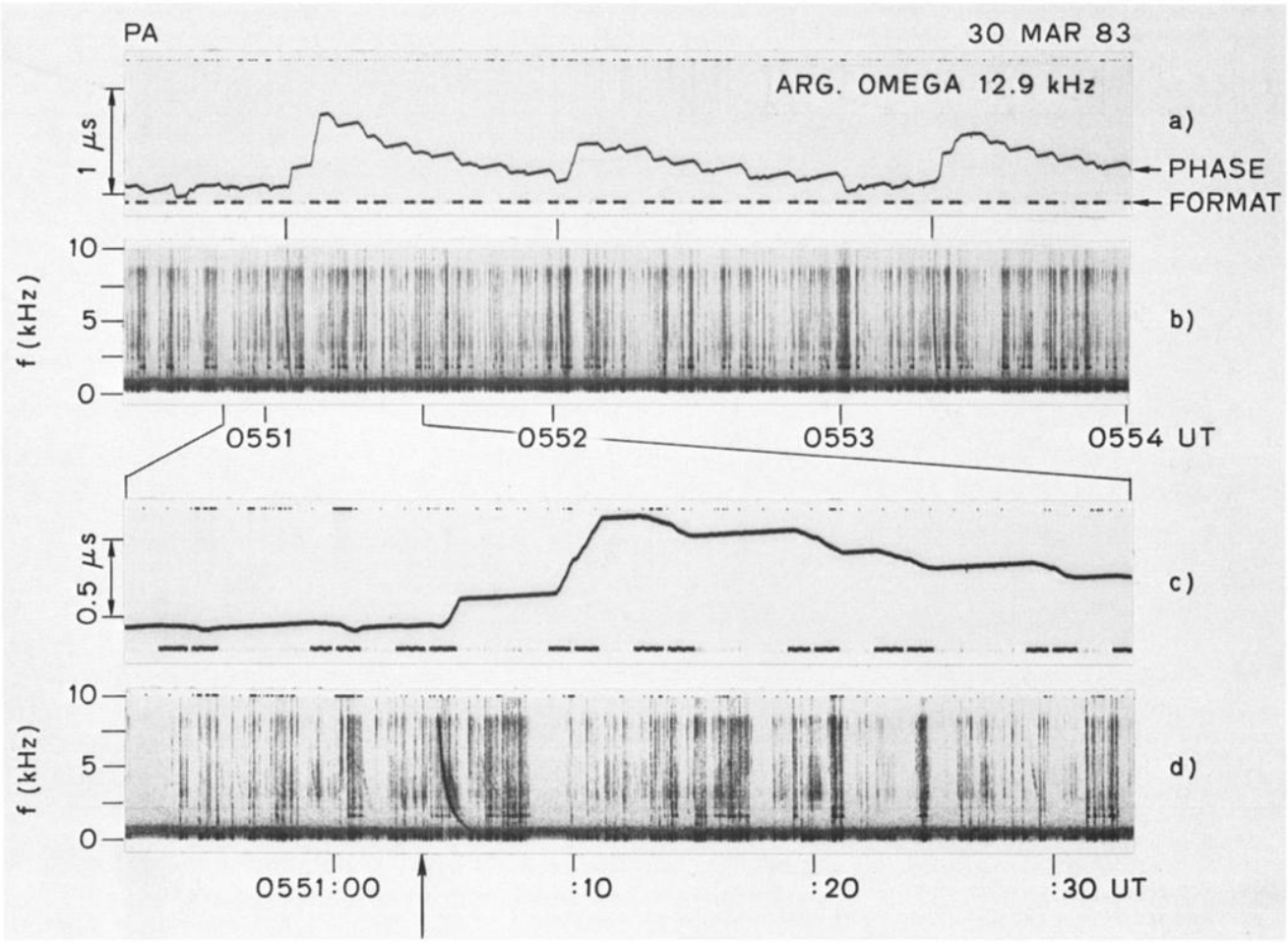

Fig. 4. The top two panels illustrate the correlation between three different 12.9-kHz phase advances and the 0- to 10-kHz frequency-time spectrum showing whistlers. The times of the events are marked with vertical bars. The top panel also shows the time format of the Omega pulses as received at Palmer. The sawtooth nature of the phase record is due to the slow drift of the phase holding circuit during the signal-off periods. The lower two panels show an expanded record of the first of the three events.

readily recognized for the events shown in Figures 3 and 4. This signature is similar to those reported for whistler-induced amplitude perturbations and can be used for identification of events. The recovery time is believed to be controlled by the attachment rate for excess ionization at 80-90 km altitude [*Dingle*, 1977].

Examples of Phase Perturbations

In this section we present examples of phase perturbations on signals from various sources. The upper and middle panels of Figure 5 show, respectively, remarkably similar amplitude and phase perturbations on 37.2-kHz LF signals (see Table 1) received at Palmer. Rapid changes are followed by relatively slow recoveries of 20–30 s. Included is a pair of closely spaced events in which the second perturbation occurs before the signal phase recovers from the first one. The bottom display of integrated intensity in the 2- to 4-kHz band shows spikes at the times of correlated whistlers.

Phase and amplitude perturbations of a 23.4-kHz signal from the VLF communication transmitter NPM (see Table 1) observed at Palmer are shown in Figure 6. The bottom panel again shows the integrated VLF intensity in the 2- to 4-kHz band. Accompanying the whistler spikes is a ~ 30-s-duration pulse at 2.45 kHz from the Siple Station experimental VLF transmitter [*Helliwell and Katsufrakis*, 1978]

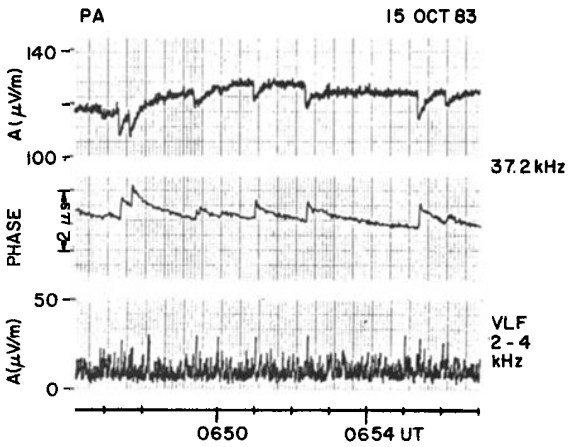

Fig. 5. Amplitude (top panel) and phase perturbations of a 37.2-kHz signal observed at Palmer. The bottom panel shows integrated intensity in the 2- to 4-kHz band.

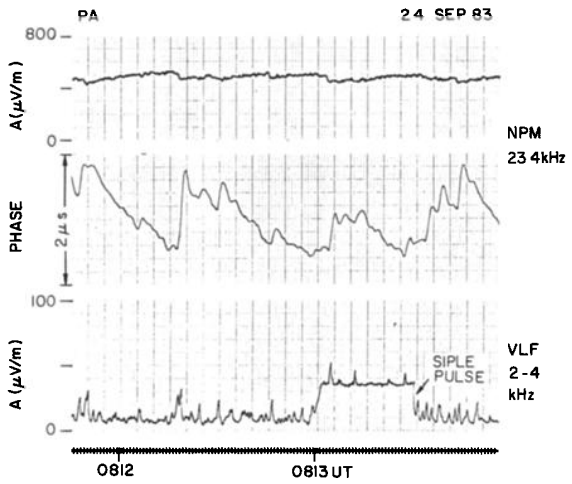

Fig. 6. Amplitude (top panel) and phase perturbations of the 23.4-kHz signal from the NPM transmitter. The ~ 30-s pulse shown on the bottom record of 2- to 4-kHz integrated intensity is due to a 2.45-kHz signal from the Siple Station (see Figure 2) experimental transmitter.

(see Figure 2), which arrives at Palmer over a subionospheric path and has no detectable effect on the observation of the NPM signal. Both the main features and the fine structure of the observed phase variations appear to be associated with magnetospheric whistlers. The amplitude variations of the NPM signal shown in the top panel are also time correlated with whistlers, but are relatively small, at the 0.05- to 0.1-dB level.

Examples of phase perturbations of the 12.9-kHz Omega Argentina signal are shown in Figures 7 and 8. Figure 7 illustrates a case in which lightning-induced phase perturbations on the 12.9-kHz signal occur simultaneously with amplitude changes on other signals with arrival bearings that extend over a ~ 90° range (see Figure 2). At other times only some of these paths may show detectable perturbations as illustrated in Figure 8. In this case, the 12.9-kHz and NSS signals, with closely spaced great circle paths near the receiver, are the only ones showing identifiable Trimpi effects.

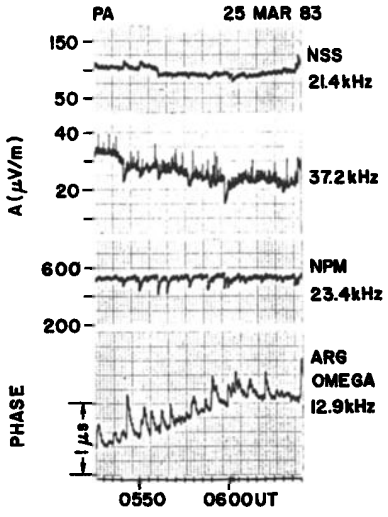

Fig. 7. Chart record from Palmer, Antarctica, showing 12.9-kHz Omega phase perturbations concurrent with amplitude perturbations on other signals (see Figure 2).

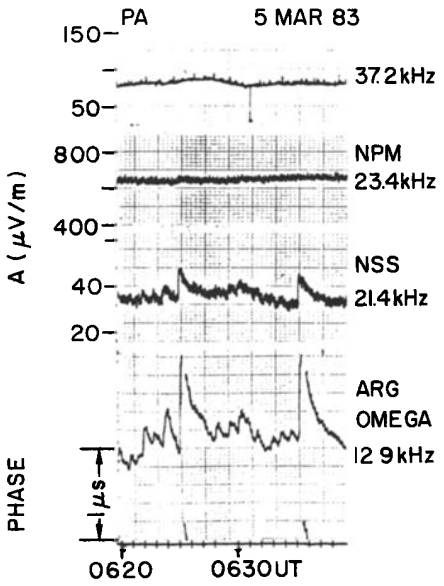

Fig. 8. Large (~1 μs) phase advances of 12.9-kHz observed simultaneously with amplitude changes on the NSS signal, with no apparent perturbations on the 37.2-kHz and NPM signals arriving over paths lying further west.

On occasions in October of 1983 the single available phase tracking receiver at Palmer was tuned to a different VLF/LF signal source at intervals of ~ 20 min, so as to study the occurrence of phase Trimpi activity as a function of path location. Figure 9 shows one of the more active cases, in which five different signals exhibited phase events. Portions of the original chart are displayed.

Occurrence Statistics

To document the occurrence patterns of whistler-induced phase perturbations we rely on measurements of the 12.9-kHz Omega Argentina signal; there is relatively good coverage in the form of chart recordings throughout the period January-July 1983, with continuous coverage of 24 hours for most days.

The seasonal variation of occurrence of phase perturbations at 12.9 kHz, defined as the number of hours per day

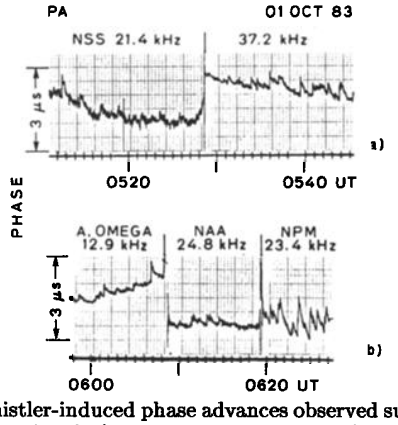

Fig. 9. Whistler-induced phase advances observed successively on five different signals (see Figure 2 and Table 1). Portions of the original chart are displayed, showing the times when the single available phase tracking receiver was switched from one source to another.

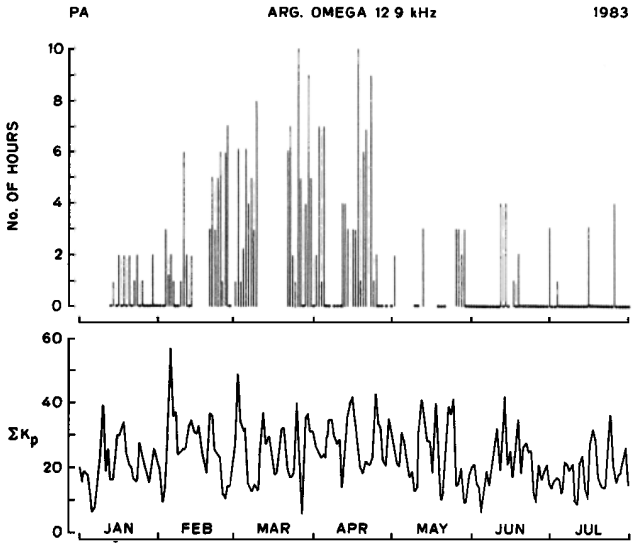

Fig. 10. The seasonal variation of the occurrence of phase perturbations at 12.9-kHz, defined as the number of hours per day during which at least one event was observed. Small circles represent days of no detectable events whereas the gaps indicate that data coverage was not complete. The lower panel shows a plot of ΣKp for the same period.

during which at least one event was observed, is shown in Figure 10. The ΣKp for the same period is plotted in the lower panel. Days on which no events were observed are shown with small circles, whereas gaps indicate that data coverage was not complete. The result shows a clear peak in occurrence rate during the March-April equinoctial period, which is consistent with a September-October equinoctial peak in VLF/LF amplitude perturbations observed at Palmer in 1978 [*Carpenter and LaBelle*, 1982].

The statistics of the number of hours per day with events and the event rate per hour during March/April 1983 are shown in Figures 11*a* and 11*b*. Figure 11*a* shows that when events did occur, they were long enduring, lasting more than 4 hours in ~50% of the cases. In Figure 11*b* the hourly rate distribution falls off rapidly at first, but is then relatively flat between ~12 and ~40 events per hour. Examples of event occurrence at high and low hourly rates are shown in Figure 12; the upper panel shows a case in which ~ 40 events per hour were observed, whereas the lower panel illustrates a case with only one detectable event during a ~ 30 min period.

Figure 11*c* indicates that most of the observed events involved phase advances of ≤ 0.3 μs, with the number of perturbations ≥ 0.6 μs being very small.

Comments on the Experimental Results

The occurrence statistics of the Argentina Omega 12.9-kHz phase perturbations are comparable to those of the amplitude perturbations on the most "active" VLF/LF signals observed at Palmer. This, plus the indications that corresponding amplitude changes on Omega were either not detected or were only marginally detectable, in the range ~0.04–0.2 dB [*Carpenter et al.*, 1984], supports the general expectation [e.g., *Lohrey and Kaiser*, 1979] that phase perturbations should exceed amplitude changes in terms of dectability.

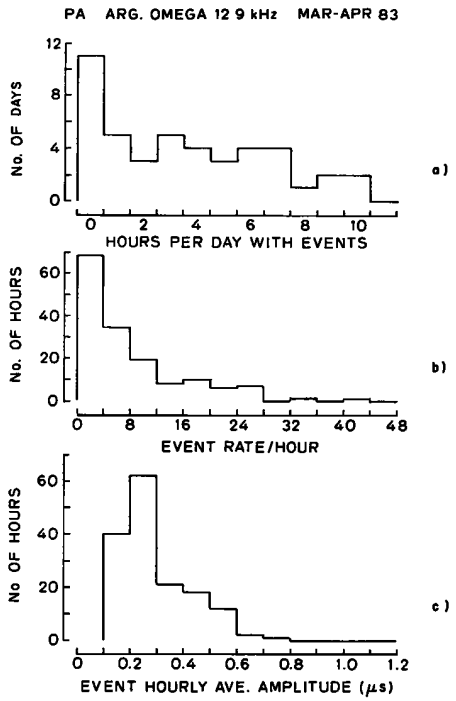

Fig. 11. Occurrence statistics of 12.9-kHz phase perturbations during March–April 1983. (*a*) Number of days versus hours per day with events, (*b*) number of hours versus event rate per hour, and (*c*) number of hours versus hourly averaged event amplitude (microseconds).

The apparent seasonal peak at the equinox has yet to be explained. The drop-off in the austral summer may in part be attributed to solar illumination, but the decrease in the austral winter must be attributed to other factors. Since Trimpi effects near L=2 are found to peak in the several-day aftermath of magnetic storms [*Carpenter and LaBelle*, 1982; *Leyser et al.*, 1984] and thus appear to depend upon radial diffusion processes following injection events, the winter decrease may be partly due to the seasonal falloff in disturbance activity, as indicated by the average ΣKp level in Figure 10 and discussed by *Russell and McPherron* [1973]. This and other possibilities are currently under investigation.

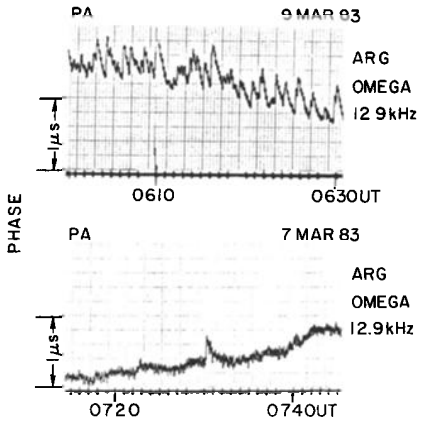

Fig. 12. Examples of different rates of occurrence of phase perturbations: (top) high occurrence rate of ~ 40 events per hour, and (bottom) a single isolated event during a ~ 30-min period.

The long enduring nature of the activity during local night suggests that in most cases the associated magnetospheric particle fluxes, presumably enhanced over levels characteristic of extended quiet times, are more or less uniformly distributed in local time.

3. Interpretive Model of an Individual Event

The whistler-induced subionospheric signal perturbations are believed to be a manifestation of the combined effects of various physical processes (see Figure 1). These include the occurrence of lightning and the coupling of its electromagnetic energy into the ionosphere; the propagation of the whistler wave in the magnetosphere; and the whistler-particle gyroresonance interaction and the wave-induced scattering of the particles; the ionospheric perturbations induced by the precipitating particles; and the disturbing effect of these perturbations on radio wave propagation in the earth-ionosphere waveguide. Each one of these steps involves important but incompletely understood physics; the extent of our understanding varies in each area.

Models of the physical processes mentioned above do exist and can be used for first-order interpretation of the observations. We can expect that further investigations of Trimpi effects will lead to substantial improvement of the models, especially in view of (1) the transient nature of the events, (2) the possibility of measuring details of the time signature of the signal changes, and (3) the fact that both the perturbations and the magnetospheric whistler can be observed simultaneously.

An important question raised by the foregoing results, and by other recent work, concerns the spatial extent of the precipitation zones. Crude estimates of the perturbation regions have been made with the aid of the relationship of the day/night terminator to the great circle paths [*Leyser et al.*, 1984], the latitude of propagation of the magnetospheric whistler as derived from its measured dispersion characteristics, and the measured arrival bearing of the correlated whistler [*Carpenter and LaBelle*, 1982]. Results showed that most events were caused by ionospheric effects occurring within $\sim$ 1000 km of Palmer Station, although some events were found to be due to precipitation regions as far as $\sim$ 1800 km from the station. In terms of the size of the regions, *Carpenter and LaBelle* [1982] concluded from direction finding data on correlated whistlers that in some cases individual ionospheric disturbances are of order $\sim$100 km in east-west extent. However, from observations of simultaneous perturbations on signals with widely different arrival bearings, *Carpenter et al.* [1984] suggested that in many cases there are multiple precipitation zones, distributed over a region of order 500 km in extent.

It is also possible that precipitation occurs with some degree of spatial continuity over large regions, say of 500-1000 km in extent. *Thomsen and Dowden* [1978] interpreted their whistler observations to imply that whistler ducts are arclike, with east-west dimensions a factor of 8-16 greater than their north-south extent. Irrespective of the effective areas of precipitation induced by ducted whistlers, it is possible that the nonducted whistler components that accompany them contribute significantly to the overall precipitation [*Voss et al.*, 1984], in which case the affected regions would tend to be larger than ground whistler analysis would suggest.

Interpretation of an Individual Phase Event; Measured Parameters

Using existing models of the various physical processes mentioned above, we now present a first-order interpretation of the whistler-induced phase perturbations of the 12.9-kHz Omega Argentina signal. The event that we choose for interpretation is shown on an expanded time scale in Figure 13. The middle panel shows a VCO trace of the 12.9-kHz phase above the indicated time of reception of a 12.9-kHz Omega pulse pair. The bottom panel shows the 0- to 10-kHz spectrum of the whistler that is associated with the phase perturbation. The time of the lightning discharge that generated the whistler is indicated by an arrow. The top panel shows a VCO record of a concurrent amplitude perturbation of the 37.2-kHz signal.

The measured parameters of this event that are used in the interpretation are (1) the $\sim$0.5-s time delay between the occurrence of the lightning stroke and the onset of the phase perturbation, (2) the whistler propagation path parameters $L \simeq 2.3 \pm 0.1$ and $N_{eq} \simeq 2100 \pm 300$ cm $^{-3}$ derived using whistler dispersion analysis, and (3) the electric field intensity of the whistler component in a 100-Hz band centered at 5 kHz, measured to be $\sim$100 μV/m.

The size of the phase perturbations appears to be $\sim$0.2 μs from Figure 13. However, due to the $\sim$1.5-s integration time the phase advance is only partially registered when the Omega pulse terminates at $\sim$ 0559:05 UT. A compressed record of the same event in Figure 4 shows that the full extent of the phase change is $\sim$0.5 μs. The determination of the "rise time" of the phase advance is complicated due to the $\sim$ 1.5-s integration time that was utilized for the phase tracking receiver. The 37.2 kHz amplitude trace (top panel) is probably a better indicator of the rise time; it is a continuous measurement and shows that the peak is reached within an interval of $\leq$1 s. Thus we conclude that the duration of the onset of the perturbation event is $\leq$1 s.

Subionospheric VLF Propagation

The propagation of subionospheric VLF/LF waves is often analyzed in terms of a sum of waveguide modes traveling in the spherical waveguide formed by the earth's surface and the lower ionosphere. For a sharply bounded isotropic ionosphere, using the phase velocity expression given by *Wait* [1959], the resulting differential phase advance Δt is given in terms of the corresponding effective change in the ionospheric reflection height Δh by

$$\Delta t \simeq -\frac{d}{c}\left[\frac{h_\circ}{2a} + C_n^2\right]\frac{\Delta h}{h_\circ} \tag{1}$$

where c is the speed of light, $a = 6371$ km is the mean radius of the earth, $h_\circ$ is the unperturbed reflection height, d is the length of the portion of the great circle path that is perturbed, λ is the wavelength, and $C_n = (n - 1/2)\lambda/2h$ for a waveguide mode of order n.

For the propagation of the 12.9-kHz signals, we assume a normal nighttime reflection height of $h_\circ \simeq 85$ km. In using (1), the important unknowns are (1) the order of the dominant mode (n) of propagation, and (2) the magnitude of d. Note that the total length of the great circle propagation path from Omega, Argentina, to Palmer station is $d_\circ \simeq 2400$ km. For such distances, the results of *Wait and Spies* [1964]

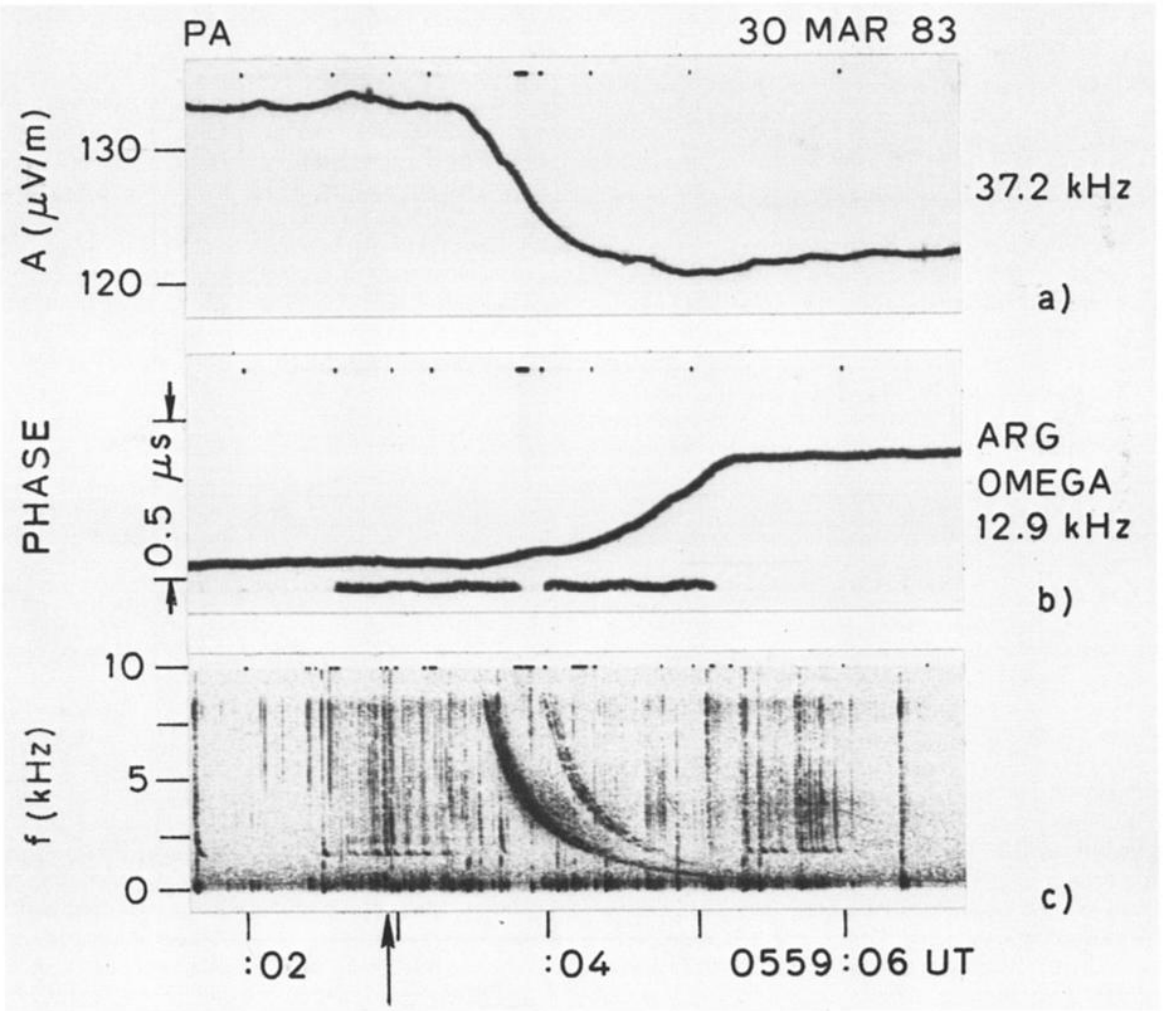

Fig. 13. Detailed correlation between a 12.9-kHz phase perturbation (middle panel) and a whistler event (lower panel) observed at Palmer station. A VCO trace for 37.2-kHz signal amplitude is shown in the top panel. The reception times at Palmer of two 12.9-kHz pulses are shown for reference at the bottom of the middle panel. A compressed record of the same event given in Figure 3 shows the full extent of the phase perturbation for this case to be ~0.5 μs.

indicate that the second mode ($n = 2$) would be dominant, due to the weak excitation of the first mode ($n = 1$) by a transmitter on the earth's surface [*Wait*, 1968] and the fact that the attenuation rates for the two modes are of the same order [*Wait and Spies*, 1964].

For whistler-induced burst precipitation events, the resulting ionospheric perturbation might be expected to be highly localized. However, as implied above, the extent of the precipitation regions is not well known. For the first-order calculation attempted here, we assume that the whistler-induced precipitation is limited to a region ~ 200 km in extent, centered ~ 200 km equatorward of Palmer. This is in reasonable agreement with the preliminary findings of *Carpenter and LaBelle* [1982] and with the measured whistler path L value.

Using n=2 and $d \simeq 200$ km in (1), we find

$$\Delta h \simeq -2.6\Delta t \tag{2}$$

where Δt is the phase change in microseconds and Δh is the height change in kilometers. For the case shown in Figure 13 and Table 1, we have $\Delta t \simeq 0.5$ μs and $\Delta h \simeq -1.3$ km.

While equation (1) assumes a sharply bounded ionosphere, we now consider an exponential ionosphere for the purpose of converting the computed height change to an enhancement of electron density. Using the notation of *Wait and Spies* [1964] we assume an ionospheric profile given by

$$\omega_r = \frac{\omega_p^2}{\nu} = \omega_{ro}\exp[\beta(h - h_o)] \tag{3}$$

where ω_p is the angular plasma frequency given by $\omega_p^2 = 3.2 \times 10^9 N_e$, with N_e being the electron number density in cm^{-3}, ν is the electron collision frequency, β is the sharpness parameter, h is the height above ground, and ω_r is the ionospheric conductivity parameter having a value of ω_{ro} at the reference unperturbed reflection height of h_o. For our calculations below, we use commonly adopted values of $\beta = 0.5$ km^{-1}, $\nu = 10^6$ s^{-1}, and $\omega_{ro} = 2.5 \times 10^5$ s^{-1} [*Wait and Spies*, 1964; *Potemra et al.*, 1967, 1969; *Lohrey and Kaiser*, 1979].

Using this model with $h_o \simeq 85$ km, and assuming that the reflection occurs at the same electron density value, we can calculate the density enhancement ΔN_e that would cor-

TABLE 1. List of Transmitters Observed at Palmer Station

Transmitter	Location	Latitude	Longitude	Frequency, kHz
NSS	Maryland	39°N	76°W	21.4
NPM	Hawaii	21°N	158°W	23.4
LF	California	35°N	117°W	37.2
MF	Argentina	50°S	69°W	780.0
Omega	Argentina	43°S	65°W	12.9
NAA	Maine	45°N	67°W	24.8

respond to a given height reduction Δh. For the $\Delta h \simeq -1.3$ km calculated above we find $\Delta N_e \simeq 37$ el/cm^3. This value is used below in comparison with the expected enhancements from precipitating particle fluxes.

We note here that equation (1) and the computation of Δh are based on a sharply bounded ionosphere model, whereas we have used an exponential ionosphere for computing the required density enhancement through (3). We use such a hybrid model due to the difficulty of estimating Δh for a given Δt in the exponential model. While parameterized curves of phase velocity as a function of frequency and for different reflection heights are available for an exponential model [*Wait and Spies*, 1964], the rate of change of phase velocity with reflection height is not easily calculated from these results. However, by scaling and interpolating from the available phase velocity curves, it can be seen that the change in reflection height for the observed phase changes is $\Delta h \simeq$1–2 km, consistent with our estimate obtained using the hybrid model.

Whistler-Particle Interaction in the Magnetosphere

For modeling the whistler-particle interaction, we utilize a test particle model of the gyroresonance wave-particle interaction in the magnetosphere [*Inan et al.*, 1982]. This model has previously been applied to the cases of interactions involving whistler waves and to direct comparisons with experimental data, including subionospheric signal amplitude perturbations [*Chang and Inan*, 1983, 1985; *Carpenter et al.*, 1984]. The model simulates the interaction of the whistler wave and the particle distribution by computing the trajectories of a large number of test particles. The propagation of the whistler signal from one hemisphere to the other in a ducted mode is assumed, and the interaction of the wave with particles of different energy as it propagates along the field line is taken into account.

The result of using this model for the path parameters L and N_{eq} estimated above is shown in Figure 14. For this calculation, we have assumed a typical quiet time isotropic trapped particle distribution with the differential energy spectrum $\Phi_E = 10^5$ el cm^{-2} s^{-1} sr^{-1} keV^{-1} for $E = 40$ keV particles [*Lyons and Williams*, 1984]. The energy dependence of the trapped distribution was assumed to be E^{-3}, not inconsistent with particle energy spectra observed at these L shells.

As for the wave parameters, the equatorial wave magnetic field derived from the measured intensity at the ground of $\sim$100 μV/m in a 100-Hz band centered at 5 kHz is estimated to be 1-10 pT. The range of values is due to the uncertainty in the distance between the duct exit point from the ionosphere and the receiver on the ground and the radiation pattern at the exit point. For a distance of $\sim$ 200 km, using a $\sim$ 7 dB/100 km attenuation as measured by *Tsuruda et al.* [1982], an ionospheric D region absorption of $\sim$ 3 dB, and accounting for the expansion of the field lines between ionospheric altitudes and the equatorial plane ($\sim$ 11 dB at $L \simeq 2.3$), we find the corresponding equatorial wave magnetic field intensity $B_w \simeq 2$ pT. However, if the duct exit point is at a distance of $\sim$ 500 km from the receiver, due to ionospheric propagation effects [see *Gorney and Thorne*, 1980; *Strangeways*, 1981] or displacement in longitude from the Palmer meridian, the estimated equatorial field intensity would be $\sim$ 20 pT. For the computations given below, we use a value of $B_w \simeq 10$ pT. The whistler wave at $t = 0$ is assumed to be a pulse with a constant power spectral density over the frequency range of 500 Hz to 10 kHz. Due to dispersion, the equatorial wave intensities at lower frequencies are smaller, with equatorial intensity being equivalent to that of a monochromatic signal of 10 pT intensity at 5 kHz.

The top panel in Figure 14 shows the energy flux versus time in ergs cm^{-2} s^{-1} as observed in the southern hemisphere, where t=0 is the time of origin of the lightning stroke that generated the whistler. The whistler is assumed to originate in the northern hemisphere and interacts with the electrons as it travels southward. The particles that are pitch angle scattered as a result of this interaction first travel to the northern hemisphere, where they mirror back due to the relatively high mirror altitudes (at longitudes near the South Atlantic magnetic anomaly). They then precipitate into the ionosphere in the southern hemisphere, where they first arrive $\sim$ 0.32 s after the lightning stroke. The computed whistler-induced precipitation pulse reaches half of its peak value at $\sim$0.5 s, consistent with the delay of $\sim$ 0.5 s measured on the records in Figure 13. The full width at half maximum of the precipitation burst is $\sim$ 0.4 s, again consistent with the inferred duration of the onset of the subionospheric signal phase perturbations. The peak energy flux level is $\sim 1.4 \times 10^{-3}$ ergs cm^{-2} s^{-1}.

The energy range of the computed flux as a function of time is shown in the lower panel of Figure 14. The whistler-induced precipitation flux consists of particles in the 40- to 250-keV energy range. As discussed in the following subsection, particles in this energy range contribute to the ionization in the ionospheric D region at altitudes of 80–90 km [*Rees*, 1969].

It should be noted here that while the assumed parameter values affect significantly the magnitude and energy spectra of the computed fluxes they have little effect on the timing relationships. Among the parameters assumed, the trapped energetic particle distribution, taken to be proportional to

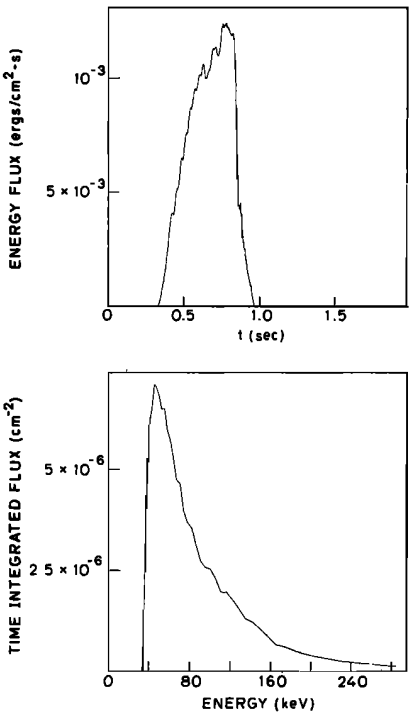

Fig. 14. Computed precipitation flux induced by a whistler propagating at $L \simeq 2.3$ and for an equatorial cold plasma density of 2100 el/cm^3. The upper panel shows the total energy flux as a function of time, while the lower panel shows the time-integrated energy spectrum of the whistler-induced precipitation burst. The whistler is assumed to cover a frequency range of 500 Hz to 10 kHz and to have entered the medium at 1000 km altitude at t=0 in the northern hemisphere. The input signal is assumed to have constant power spectral density over the frequency range 500 Hz to 10 kHz, so that the equatorial wave intensity at lower frequencies is smaller due to higher dispersion. The equatorial wave magnetic field intensity at 5 kHz was taken to be 10 pT. The energetic particle distribution was taken to be proportional to E^{-3}, where E is the particle energy. The differential energy spectrum for 40-keV particles was assumed to be 10^5 el cm^{-2} s^{-1} sr^{-1} keV^{-1}.

E^{-3}, determines the relative amounts of flux at various particle energies. The magnitude of the energy flux in ergs cm^{-2} s^{-1} is directly proportional to the trapped flux level Φ_E near the edge of the loss cone as well as the wave magnetic field intensity. For an assumed Φ_E at, for example, E=40 keV, the peak flux level also depends strongly on the energy dependence of the distribution function, with the peak flux for an E^{-1} dependence being as much as an order of magnitude larger than that for E^{-3} at $L \simeq 2.3$. On this basis, and in the absence of information on the energy dependence, the peak flux level computed using this model is in the range 10^{-3}–10^{-2} ergs cm^{-2} s^{-1} [*Chang and Inan*, 1985].

Ionospheric Effects of Whistler-Induced Precipitation Bursts

In order to estimate the secondary ionization that would be produced by the whistler-induced flux in the lower ionosphere we use the results of *Rees* [1969]. For isotropic streams of monoenergetic precipitating electrons, the ion pair production rate at the D region altitudes of $\sim$ 85 km is found to be $\sim 10^{-3}$ cm^{-3} s^{-1} per unit incident electron flux in cm^{-2} s^{-1}, for electrons in the 40- to 250-keV range.

Using this approximate value, and considering an average particle energy of $\sim$ 100 keV, we can estimate the precipitating electron flux that would be required in order to produce a density enhancement of $\Delta N_e \simeq 37$ cm^{-3} during the computed $\sim$ 0.5-s duration of the whistler-induced precipitation burst. The result is a flux of $\sim 10^{-2}$ ergs cm^{-2} s^{-1} of 40- to 250-keV electrons.

Due to the above mentioned uncertainties in the trapped particle distribution and the whistler wave intensity, it is not possible to make an accurate comparison of this value with that computed above. However, it is encouraging to note that the two results are comparable on an order of magnitude basis. More importantly, the required flux of $\sim 10^{-3}$–10^{-2} ergs cm^{-2} s^{-1} is consistent with the whistler-induced energetic electron fluxes that were directly observed on a low-altitude satellite [*Voss et al.*, 1984].

Interpretation of Other Phase Events

While the above calculations apply to the specific case of the individual event shown in Figure 13, the method can be applied to the other cases shown in this paper. Previous work on amplitude perturbations at Palmer has shown that the L shell of propagation for the perturbing whistler is usually in the L=2–2.4 range [*Carpenter and LaBelle*, 1982]. From Figure 11*c*, we note that a phase change of $\sim$0.2 μs is more typical than the $\sim$0.5 μs in the case of the event shown in Figure 13. For $\Delta t \simeq 0.2$ μs, and for $h \simeq 200$ km, we find from (2), $\Delta h \simeq -0.52$ km, which in turn corresponds to a density enhancement of $\sim$ 31 el/cm^3.

The overwhelming majority of the whistler-induced phase perturbations observed on the 12.9-kHz Omega Argentina signal were positive changes (i.e., phase advances). However, a few cases of negative changes were also observed. In the context of the interpretation provided here, a reduction in effective ionospheric reflection height would always lead to phase advances. However, phase delays may result from changes in the height gradient of electron density at the reflection altitude. This might be caused by whistler-induced precipitation of particles within a limited range of energies such that the height gradient is changed without significant reduction in reflection height.

Discussion of the Interpretive Model

We have presented a first-order quantitative interpretation of the observed whistler-induced VLF/LF phase perturbations, attempting to connect the various physical processes that occur during such events. A quantitative interpretation of the observed perturbations is needed in order to realize the potential of VLF/LF phase measurements as a means of detecting and measuring wave-induced burst precipitation. We realize that our first-order model is far from comprehensive and involves many approximations.

Among the important assumptions that were made above is the choice of d, i.e., the length of the portion of the propagation path that is perturbed. For example, a value of d = 100 km would result in a height change $\Delta h \simeq -2.6$ km, which in turn would correspond to a density enhancement of $\Delta N_e \simeq 56$ cm^{-3}. This would then require an incident particle flux that is $\sim$ 1.5 times larger. Thus it seems that

the determination of the spatial size of the perturbed ionospheric regions is important for quantitative interpretation of the results. In the same connection, the effects of perturbations that are not located directly on the great circle path must be recognized. Using data on arrival bearings of whistlers, *Carpenter and LaBelle* [1982] found that the centers of precipitation regions could be as much as ~200 km from the affected great circle paths. Furthermore, if the perturbations of the waveguide are located near the receiving station, the single mode theory employed here may not be applicable, and a full wave solution may be required.

In the modeling of the whistler-particle interaction we computed the precipitated flux induced by a single whistler component propagating in the ducted mode along the earth's magnetic field. The same lightning discharge that launches such a whistler would also be expected to generate nonducted wave components that may not be observed on the ground. The precipitation induced by these components must be considered in a more comprehensive study.

The fluxes computed using the test particle model are directly proportional to the high-altitude wave magnetic field intensity and the trapped flux level: quantities that were not measured explicitly during the experiments. Wave intensity was inferred from the ground-based measurement, but not without significant ($\geq$ 10 dB) uncertainty as discussed above. The perpendicular electron flux for trapped particles of $\sim$ 40 keV energy was taken to be 10^5 el cm^{-2} sr^{-1} s^{-1} keV^{-1}, but for $L \simeq 2.3$ this quantity can vary over a range of $10^4 - 10^6$ [*Lyons and Williams*, 1984]. Furthermore, the particle distribution was assumed to be isotropic, whereas at times the flux near the edge of the loss cone at the equatorial plane can be as much as an order of magnitude lower than the perpendicular flux.

The relative sensitivity of VLF phase versus other techniques (e.g., riometer) for detecting D region ionization was previously discussed in the context of diurnal phase variations and substorm-related effects [*Potemra et al.*, 1969; *Potemra and Rosenberg*, 1973]. However, these studies were mostly based on steady state considerations, comparing, for example, the ion pair production rate due to precipitating electrons to other sources for nighttime ionization. The relatively short duration of the burst precipitation events implies that these arguments may not be directly applicable, since all of the extra ionization needed for the lowering of the effective ionospheric reflection height must be produced during a short time. Thus the incident particle fluxes should tend to be higher for such events. In any case, further theoretical and experimental work is needed for assessing the feasibility of using phase measurements for quantitative measurement of burst precipitation of the radiation belt particles.

4. Possible Effects on Global VLF/LF Navigation

Apart from their geophysical significance, the VLF/LF phase perturbations discussed above may have an effect on global navigation and communication systems that rely on phase coherent subionospheric transmissions. In this section, we briefly discuss such possible effects.

The importance of global navigation systems was emphasized by a recent special issue of the *Proceedings of the IEEE* on this topic [*Dodington*, 1983]. Prominent among the systems that are currently in use are the Omega and LORAN-C systems, which are based on long-range hyperbolic navigation involving, respectively, the measurement of phase and time differences among signals from selected VLF/LF transmitters located around the globe [*Swanson*, 1983; *Frank*, 1983]. The effects of impulsive noise from atmospheric lightning within the operating frequency range of, for example, the Omega system (10.2–13.6 kHz) have long been recognized. Such effects are caused by lightning-induced electromagnetic wave energy that propagates in the earth-ionosphere waveguide and are somewhat random in occurrence. In contrast, the effect of the lightning-induced particle precipitation events has a rather characteristic temporal signature in the form of perturbations of the earth-ionosphere waveguide that occur repeatedly near the conjugate ends of field-aligned magnetospheric paths. The geographic distribution of such effects would depend on the distribution of thunderstorm regions as well as other geophysical parameters such as the distribution of the trapped radiation flux.

While the overall effect of this phenomenon in global navigation may or may not be significant, such effects undoubtedly occur and may contribute to the overall error margin of the system [*Swanson*, 1983]. In terms of effects on navigation, it is important to recognize that the burst precipitation events tend to be localized in longitude and latitude as a result of the localized nature of the causative lightning discharge. Thus, in the frame of an observer using a global navigation system such as Omega, it is likely that only one of any two monitored signal paths would be affected. This in turn would enhance the likelihood of a navigational error. In the following we discuss possible effects of these phase perturbations on the Omega and LORAN-C navigation systems.

The Omega Navigation System

Assuming that wave propagation speed in the earth-ionosphere waveguide is roughly equal to the speed of light, a ~1 μs phase shift corresponds to a 300-m or $\sim$ 0.16-nmi (nautical miles) change in the apparent source-to-receiver distance. Depending on the location of the signal sources with respect to a receiver, this may translate directly into a position error, particularly when only one of the two or more received signal paths is perturbed. When compared with the 1–4 km realizable fix accuracy of the Omega system [*Swanson*, 1983], the effect of typical lightning-induced phase changes shown in this paper would seem to be small. On the other hand, effects of such perturbations may be significant in the use of Differential Omega systems that are employed for increased accuracy and that are based on the assumption that propagation disturbances affect both paths in a similar manner [*Beukers*, 1973]. Also, the class of fast phase changes that occur at higher latitudes, poleward of $\sim 60^\circ$ magnetic latitude, appears to involve delays that are much larger, of order ~10 μs [*Carpenter et al.*, 1985]. These should be of significance to system users in high-latitude regions.

In any case, it should be noted that the phase perturbations have a characteristic signature and are unidirectional at any given time. Thus, fix accuracy may be increased by monitoring the phase of the various signals, ignoring those that exhibit such variations, and relying on redundant non-

perturbed paths for navigation. Automatic recognition of and correction for such errors may be possible.

The LORAN-C Radio Navigation System

The LORAN-C system currently operates in the 90- to 110-kHz band, using short radio frequency pulses and relying on measurement of the time difference between signals from a master station and secondary station(s) [*Frank*, 1983].

The whistler-induced phase (or travel time) perturbations for such signals were not monitored during the Palmer experiments. However, the facts that (1) phase perturbations were observed on signals with frequencies up to 37.2 kHz, with typical changes being the same as those for 12.9-kHz signals, and (2) lightning-induced amplitude perturbations were observed on signals with frequencies as high as 800 kHz [*Carpenter et al.*, 1984], suggest that similar perturbations occur on signals in the ~100-kHz range. Observations of 100-kHz LORAN-C signals propagating over relatively short paths (1500 to 4000 km) at mid- to low latitudes in the northern hemisphere were carried out by *Doherty* [1971]. While the possible association with whistler waves was not recognized, the results obtained were remarkably similar to the VLF/LF signal perturbations presented above. Rapid simultaneous amplitude and phase perturbations were frequently observed, with a clear peak in occurrence during equinoctial periods.

The predictable accuracy of the LORAN-C navigation system is believed to be better than ~ 500 m, with a repeatable accuracy of 18–90 m. In some cases, an absolute accuracy of 30 m was achieved even with very high radio interference levels [*Frank*, 1983]. In view of this, and assuming that the phase perturbations on the ~ 100-kHz signals can be expected to be similar to those shown in this paper, the lightning-induced phase changes of 0.1–1 μs corresponding to distance errors of 30–300 m would seem to be significant. Thus it is possible that whistler-associated phase perturbations may be an important source of error for the LORAN-C system.

5. Concluding Remarks

We have presented new evidence of phase perturbations of VLF/LF subionospheric signals caused by whistler-induced burst particle precipitation from the magnetosphere. Phase advances of 0.1–1.0 μs on a 12.9-kHz signal arriving at Palmer, Antarctica ($L \sim 2.3$), over a ~ 2400-km path are regularly observed with a characteristic signature of a rapid ($\leq$ 1-s) onset followed by a relatively slow (10- to 30-s) recovery. Event occurrence peaks during equinoctial periods, with typical rates of 1–40 events per hour lasting for several hours per night. Examples have also been observed at Palmer on VLF/LF signal paths that are distributed over a ~ 90° range in arrival bearing. The magnitude of the observed phase perturbations seems to be comparable to the fix accuracy of some global navigation systems that rely on phase coherent subionospheric transmission.

A first-order interpretation of an individual event has been developed, including the whistler-particle interaction in the magnetosphere, the secondary D region ionization that is generated by the wave-induced precipitation flux, and resulting effects on the subionospheric propagation of the radio waves. The observed phase perturbations correspond to a rapid reduction of up to ~1 km in the effective nighttime ionospheric reflection height (~85 km) for the subionospheric VLF signals. Results indicate that the incident energetic particle fluxes that are required to produce the extra ionization are reasonably consistent with those estimated using theoretical models of the whistler-particle interaction as well as direct satellite-based observations.

Generally the results suggest that measurement of the phase of subionospheric VLF/LF signals can potentially be useful as a tool for studying wave-induced burst particle precipitation from the magnetosphere.

Acknowledgments. We thank M. Trimpi for his work at Palmer Station and our colleagues at the STAR Laboratory for their support. We also thank J. Yarbrough and P. Pecen for their assistance in data analysis and display. The typescript was prepared by N. Leger. This work was supported by the Division of Polar Programs of the National Science Foundation under grants DPP-82-17820 and DPP-80-22282 and by the National Aeronautics and Space Administration under grant NGL-05-020-008.

The Editor thanks H. C. Koons and R. L. Dowden for their assistance in evaluating this paper.

References

Beukers, J. M., Accuracy limitation of the OMEGA navigation system employed in the differential mode, *Navigation, 20,* 81, 1973.

Brice, N., Fundamentals of VLF emission generation mechanism, *J. Geophys. Res., 69,* 4515, 1964.

Carpenter, D. L., and J. W. LaBelle, A study of whistlers correlated with bursts of electron precipitation near L=2, *J. Geophys. Res., 87,* 4427, 1982.

Carpenter, D. L., U. S. Inan, M. L. Trimpi, R. A. Helliwell, and J. P. Katsufrakis, Perturbations of subionospheric LF and MF signals due to whistler-induced electron precipitation bursts, *J. Geophys. Res., 89,* 9857, 1984.

Carpenter, D. L., U. S. Inan, E. W. Paschal, and A. J. Smith, A new VLF method for studying burst precipitation near the plasmapause, *J. Geophys. Res., 90,* 4383, 1985.

Chang, H. C., and U. S. Inan, A theoretical model study of observed correlations between whistler mode waves and energetic electron precipitation events in the magnetosphere, *J. Geophys. Res., 88,* A12, 10053, 1983.

Chang, H. C., and U. S. Inan, Lightning-induced electron precipitation from the magnetosphere, *J. Geophys. Res., 90,* 1531, 1985.

Cornwall, J. M., Scattering of energetic trapped electrons by very-low-frequency waves, *J. Geophys. Res., 69,* 1251, 1964.

Dingle, B., and D. L. Carpenter, Electron precipitation induced by VLF noise bursts at the plasmapause and detected at conjugate ground stations, *J. Geophys. Res., 86,* 4597, 1981.

Dodington, S. H., Navigation – An overview, *Proc. IEEE, 71,* 1125, 1983.

Doherty, R. H., Observations suggesting particle precipitation at latitudes below 40°N, *Radio Sci., 6,* 639, 1971.

Dungey, J. W., Loss of Van Allen electrons due to whistlers, *Planet. Space Sci., 11,* 591, 1963.

Frank, R. L., Current developments in LORAN-C, *Proc. IEEE, 71,* 1127, 1983.

Gorney, D. J., and R. M. Thorne, A comparative ray-trace study of whistler ducting processes in the earth's plasmasphere, *Geophys. Res. Lett., 7,* 133, 1980.

Helliwell, R. A., Generation of VLF radio noise in the ionosphere by energetic particle streams, *Space Research V,* North Holland, Amsterdam, 1965.

Helliwell, R. A., and J. P. Katsufrakis, Controlled wave-particle interaction experiments, in *Upper Atmosphere Research in Antarctica, Antarctic Res. Ser. vol.* 29, edited by L. J. Lanzerotti and C. G. Park, p. 100, AGU, Washington, D. C. 1978.

Helliwell, R. A., J. P. Katsufrakis, and M. L. Trimpi, Whistler-induced amplitude perturbation in VLF propagation, *J. Geophys. Res., 78,* 5515, 1973.

Imhof, W. L., J. B. Reagan, E. E. Gaines, and D. W. Datlowe, The L shell region of importance for waves emitted at ground level as a loss mechanism for trapped electrons $\geq$68 keV, *J. Geophys. Res., 89,* 10827, 1984.

Inan, U. S., T. F. Bell, and H. C. Chang, Particle precipitation induced by short-duration VLF waves in the magnetosphere, *J. Geophys. Res., 87,* 6243, 1982.

Kikuchi, T., and D. S. Evans, Quantitative study of substorm associated VLF phase anomalies and precipitating electrons on November 13, 1979, *J. Geophys. Res., 88,* 871, 1983.

Leyser, T., U. S. Inan, D. L. Carpenter, and M. L. Trimpi, Diurnal variation of burst precipitation effects on subionospheric VLF/LF signal propagation near L=2, *J. Geophys. Res., 89,* 9139, 1984.

Lohrey, B., and A. B. Kaiser, Whistler-induced anomalies in VLF propagation, *J. Geophys. Res., 84,* 5121, 1979.

Lyons, L. R., and D. J. Williams, *Quantitative Aspects of Magnetospheric Physics,* D. Reidel, Hingham, Mass., 1984.

Potemra, T. A., and T. J. Rosenberg, VLF propagation disturbance and electron precipitation at mid-latitudes, *J. Geophys. Res., 78,* 1572, 1973.

Potemra, T. A., A. J. Zmuda, C. R. Haave, and B. W. Shaw, VLF phase perturbations produced by solar protons in the event of February 5, 1965, *J. Geophys. Res., 72,* 6077, 1967.

Potemra, T. A., A. J. Zmuda, C. R. Haave, and B. W. Shaw, VLF phase disturbance, HF absorption and solar protons in the events of August 28 and September 2, 1966, *J. Geophys. Res., 74,* 6444, 1969.

Rees, M. H., Auroral electrons *Space Sci. Rev., 10,* 413, 1969.

Russell, C. T., and R. L. McPherron, Semiannual variation of geomagnetic activity, *J. Geophys. Res., 78,* 92, 1973.

Strangeways, H. J., Determination by ray-tracing of the regions where mid-latitude whistlers exit from the lower ionosphere, *J. Atmos. Terr. Phys., 43,* 231, 1981.

Swanson, E. R., Omega, *Proc. IEEE, 71,* 1140, 1983.

Thomsen, R. J., and R. L. Dowden, Ionospheric whistler propagation, *J. Atmos. Terr. Phys., 40,* 215, 1978.

Tsuruda, K., S. Machida, T. Terasawa, A. Nishida, and K. Maezawa, High spatial attenuation of the Siple transmitter signal and natural VLF chorus observed at ground-based chain stations near Roberval, Quebec, *J. Geophys. Res., 87,* 742, 1982.

Voss, H. D., W. L. Imhof, J. Mobilia, E. E. Gaines, M. Walt, U. S. Inan, R. A. Helliwell, D. L. Carpenter, J. P. Katsufrakis, and H. C. Chang, Lightning induced electron precipitation, *Nature,* 312, 740, 1984.

Wait, J. R., Diurnal change of ionospheric heights deduced from phase velocity measurements at VLF, *Proc. IRE,* 998, 1959.

Wait, J. R., Recent theoretical advances in the terrestrial propagation of VLF electromagnetic waves, *Adv. Electron. Electron Phys., 25,* 145, 1968.

Wait, J. R., and K. P. Spies, Characteristics of the earth-ionosphere waveguide for VLF radio waves, *U.S. NBS Tech. Note, 300,* Dec. 30, 1964.

Westerlund, S., and F. H. Reder, VLF propagation at auroral latitudes, *J. Atmos. Terr. Phys., 35,* 1453, 1973.

D. L. Carpenter, R. A. Helliwell, U. S. Inan, and J. P. Katsufrakis, STAR Laboratory, Stanford University, Stanford, CA 94305.

(Received February 18, 1985;
revised April 9, 1985;
accepted April 10, 1985.)